DANISH METEOROLOGICAL INSTITUTE

TECHNICAL REPORT

98-18

Monthly Arctic Sea Ice Signatures for use in Passive Microwave Algorithms

December 1998

Søren Andersen

ISSN 0906-897X

Summary

The present report describes the determination of a set of monthly tiepoints for use in sea ice retrieval by passive microwave radiometry. From archived DMSP F-13 SSM/I data from 1996 and 1997 as well as surface temperatures from the NCEP reanalysis, emissivities are computed and analysed on a 250x250 km grid. The results are sets of monthly tiepoints for First Year ice and Open Water extracted over the Arctic Ocean, the Baffin Bay and the Baltic as well as a set of monthly tiepoints for Multi Year ice valid for the Arctic Ocean. The tiepoints cover the 19V, 19H, 37V, 37H, 85V and 85H channels. The tiepoints over open water are found from Radiative Transfer simulations to be consistent with water vapour and wind climatology. Due to this and the use of emissivity the tiepoints support the use of auxiliary data to eliminate surface temperature and atmospheric influences. Geographical differences between the Arctic and the Baffin Bay are small for the 19 and 37 GHz channels. The differences at 85 GHz in specific and between the Baltic and the Arctic in general are substantial. In the two year data set interannual variation in emissivity is largest in the summer months over Multi Year ice (up to 0.06) while typical differences are 0.01. The analysis reveals large variations in the 85 GHz signature over Multi Year ice, that complicate ice type determination by the use of these channels.

List of contents

1. Introduction

Satellite remote sensing of sea ice based on passive microwave radiation is attractive due to the large contrast in radiation between the open and the ice covered ocean surfaces as well as the relatively low sensitivity to atmospheric water content and clouds [e.g. Wilheit et al., 1972]. Starting in the early 1970's with the Electrically Scanning Microwave Radiometer (ESMR) successive series of satellites have carried microwave radiometers providing comparable measurements. Since 1987 the Special Sensor Microwave Imager (SSM/I) on board the Defense Meteorological Satellite Programme (DMSP) series has provided measurements of V and H polarised microwave radiation at the frequencies 19, 37 and 85 GHz as well as 22 GHz V polarised. The upcoming Advanced Microwave Scanning Radiometer (AMSR) and Special Sensor Microwave Imager Sounder (SSMIS) instruments will continue this heritage and even add new channels.

Algorithms for the conversion of satellite observed brightness temperatures into ice concentrations have been proposed by numerous workers since the single frequency, single polarisation algorithm for ESMR that allowed the estimation of concentrations of two radiometrically distinct surface types [e.g. Zwally et al., 1983; Parkinson et al., 1987]. With the channels featured by the SSM/I it is possible to account for 3 radiometrically distinct surfaces, which enables reasonably unambiguous estimates of arctic multiyear (MY) and firstyear (FY) ice concentrations during the winter season [Comiso, 1986; Rothrock et al., 1988; Wensnahan et al., 1993]. In order to achieve this it is necessary to provide typical emissivities, commonly referred to as tie-points, of the pure type surfaces i.e. FY, MY and open water (OW). Errors and inconsistencies in the estimated ice concentrations may arise when deviations from the tie-point emissivities occur over time due to e.g. melting, snow cover and wind roughening of the ocean surface as well as spatially due to geographical differences in chemical and physical conditions [Comiso, 1983; Eppler et al., 1992]. The use of local and seasonal tie-points has been reported to improve the accuracy and consistency of the concentration estimates significantly [Steffen & Schweiger, 1991; Thomas, 1993].

Following these recommendations, this report describes the generation of a monthly set of tie-points for the Arctic including all surface viewing SSM/I channels based on archived SSM/I data and NCEP reanalysis surface temperature fields from 1996 and 1997. It is intended for use in the algorithms developed and adapted within the context of the EUMETSAT Satellite Application Facility (SAF) on Ocean and Sea Ice. However, it is anticipated that it will be useful in other applications as well.

2. Theory

At the frequencies considered here the radiation in terms of brightness temperature of a surface is related linearly to the physical temperature of the radiating portion of the surface:

$$T_B(\lambda, p) = e(\lambda, p)T_S \qquad (1)$$

where e is an effective emissivity depending on the average electrical properties of the surface, λ is the frequency, p is polarisation (vertical or horizontal in this case) and T_S is the effective surface temperature of the radiating portion of the surface. The effective emissivity of the open ocean water (OW) is influenced by wind induced surface roughening effects [Wentz, 1983]. The emissivity of the calm ocean surface is strongly polarised but generally low, while increasing and less polarised with increasing surface roughness.

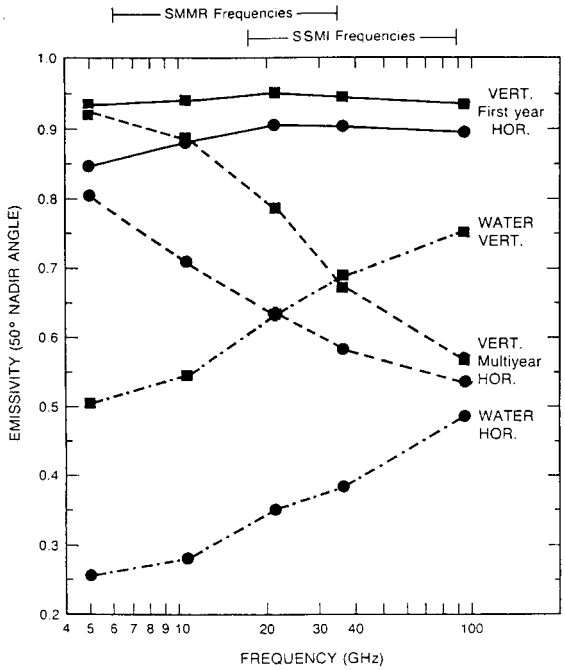

Fig. 1: In-situ Emissivities of FY, MY and OW measured during the Norwegian Remote Sensing Experiment (NORSEX) North of Svalbard during late September till early October 1979. After Svendsen et al., 1983)

The emissivity of sea ice undergoes a complex transition while forming from open water gradually thickening [Comiso, 1983] such that first year ice (FY), which is ice of approx. 0.1-2 m thickness that has not undergone a summer melt and freeze cycle, is characterised by a very high emissivity with low polarisation, whereas multi year ice (MY), i.e. ice that has survived at least one summer melt, is characterised by an emissivity declining with increased frequency and lower than FY due to airpockets formed during the summer melt, see Figure 1. To represent these characteristics and reduce the effects of physical temperature, the Polarisation Ratio (PR) and the Gradient Ratio (GR) are often defined [e.g. Cavalieri et al., 1993]:

$$PR_\lambda = \frac{T_B(\lambda,V) - T_B(\lambda,H)}{T_B(\lambda,V) + T_B(\lambda,H)}$$
$$GR_{\lambda_1\lambda_2 p} = \frac{T_B(\lambda_2,p) - T_B(\lambda_1,p)}{T_B(\lambda_2,p) + T_B(\lambda_1,p)} \qquad (2)$$

with the same notation as earlier. PR_{19} is practically insensitive to ice type variations, it is small over ice and large over open water. GR_{1937V} reflects the sensitivity to frequency of MY ice and OW such that $GR_{1937V} < 0$ for MY ice and $GR_{1937V} > 0$ for OW and $GR_{1937V} \approx 0$ for FY ice. In addition to these surface types numerous other ice types, e.g. new ice, may be found having different radiational properties. However, with the set of channels and resolution featured on presently operating satellite systems it is not feasible to distinguish them from a mixture of MY, FY and OW [Wensnahan et al., 1993]. The emissivity of the consolidated ice sheet additionally varies considerably during the meltseason due to wetness of the snowcover and due to the formation of meltponds. The former effect brings about a particularly large increase in the emissivity of the MY ice attaining values very close to that of FY.

The radiation received by the SSM/I sensor consists of contributions from the surface as given by equation 1 minus the atmospheric attenuation as well as contributions from the atmosphere and from space. This can be described by a radiative transfer equation:

$$T_B(\lambda,p) = e(\lambda,p)T_S e^{-\tau(\lambda)} + T_{B,up}(\lambda) + [1-e(\lambda,p)]T_{B,down}(\lambda)e^{-\tau(\lambda)} + [1-e(\lambda,p)]T_{B,sp}(\lambda)e^{-2\tau(\lambda)} \qquad (3)$$

where $T_{B,up}$ and $T_{B,down}$ denote upwelling and downwelling atmospheric radiation, $T_{B,sp}$ is the radiation from space and τ is the atmospheric opacity. For the rain free atmosphere, the Rayleigh criterion is applicable, i.e. scattering effects are negligible, up to 50 GHz (Ulaby et al., 1981). Furthermore, under Arctic conditions, the water content of the atmosphere is small and the attenuation is therefore small. Under rainy conditions or at frequencies above 50 GHz, however, scattering effects are important and give rise to increased atmospheric absorption as well as emission.

In the retrieval of ice parameters from satellite passive microwave radiometry, the atmospheric contributions are relatively small over the bright FY ice surfaces and most notably result in spurious ice concentrations over the open ocean as well as deficient MY concentrations. As a response to problems with spurious ice, simple thresholding filters to reject spurious pixels have been applied [Gloersen & Cavalieri, 1986; Cavalieri et al., 1995]. A more physically based approach is to retrieve atmospheric parameters (surface wind, liquid water path and integrated water vapour) from the SSM/I brightness temperatures over water and correct for them [Heygster et al., 1996]. Within the present project the use of Numerical Weather Prediction (NWP) model fields for a similar correction scheme will be described in a coming report.

Previous studies on tiepoints [e.g. Pedersen, 1991; Thomas, 1993] have often concentrated on enhancing specific aspects like bias or interannual consistency in ice concentration retrivals. Others [e.g. Svendsen et al., 1983] have based their tiepoints on field measurements of emissivity (see Figure 1), which is physically superior. However, monthly data to account for the full annual cycle are not available and it is difficult to assure representativity of the in-situ samples. Furthermore, the use of the atmospheric correction scheme mentioned

above and the more rigorous accounting for terms 1, 2 and 3 of equation 3, supports a different emphasis in the definition of tie-points. Thus, in the following tiepoints are taken to be typical emissivities characterising the individual surface type including the effect of a mean climatological (well-known) atmospheric state. In summary the objective is therefore to establish a data set that reflects the average monthly variation in surface emissivity plus atmospheric contributions. Hence, the possibility in a subsequent algorithm definition to account for surface temperature variations and atmospheric influences explicitly by means of auxiliary data is kept open.

3. Data and Methodology

3.1 Data

The present analysis is executed on a 250x250 km (10 by 10 SSM/I gridpoints) grid. DMSP F-13 SSM/I data from 1996 and 1997 are obtained from National Snow and Ice Data Center daily brightness temperature grids [NSIDC, 1996] and emissivity is calculated using daily mean surface temperature analyses from the NCEP Reanalysis. The reanalysis data are generated from NWP model reruns using advanced assimilation and data quality control schemes and are thought to represent the best possible estimate of surface temperature. Analysis confirms the data to be quite stable with small day to day variations. To convert the surface temperature to the effective temperature of the radiating ice volume, the linear relation by Svendsen et al., 1983 is used over ice. Finally, monthly histograms over ocean and ice of emissivity as well as PR_{19} and GR_{1937V} are calculated in each 250x250 km gridcell with no averaging. To that end the 25 km resolution landmask shown in Figure 2 (in grey) is used.

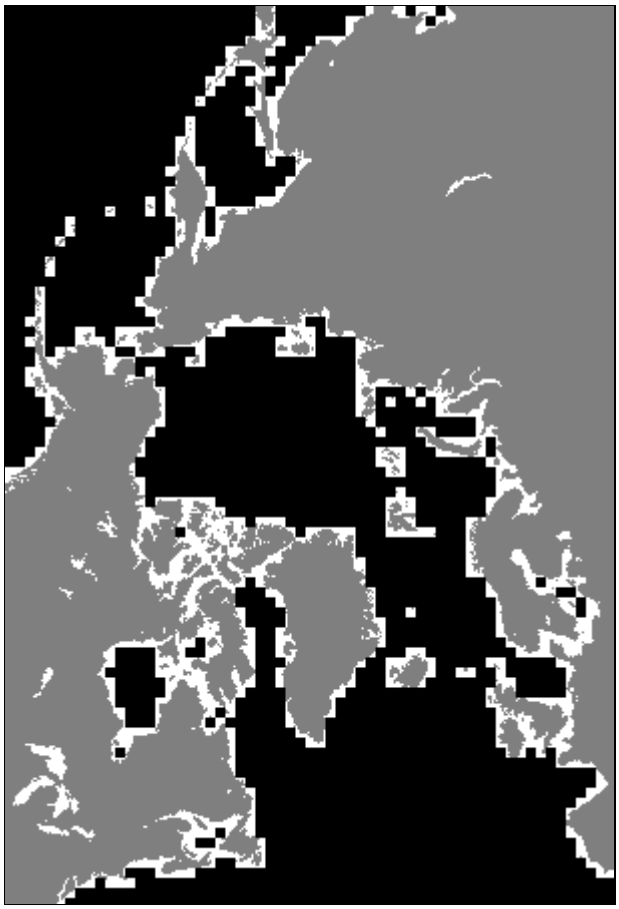

Fig. 2: Landmasks and grid definition used in the present study. The 25x25 km resolution landmask (grey) is used in computing monthly histograms. The coarse landmask (white) corresponding to the 250x250 km grid is additionally used in the manual analysis and excludes areas at risk of land contamination.

3.2 Method

Based on the 250x250 km resolution data set a manual analysis is performed. In order to avoid artefacts from land contamination the 250x250 km landmask shown in Figure 2 (in white) is applied. Almost the entire Baltic is covered by the coarse landmask, hence special care must be taken there to avoid artefacts. Figure 3 illustrates the use of histograms for extraction of tiepoints. In most channels there is sufficient separation to easily discern the peaks associated with different surface types. The specifics of the procedure for each surface type is given in the following.

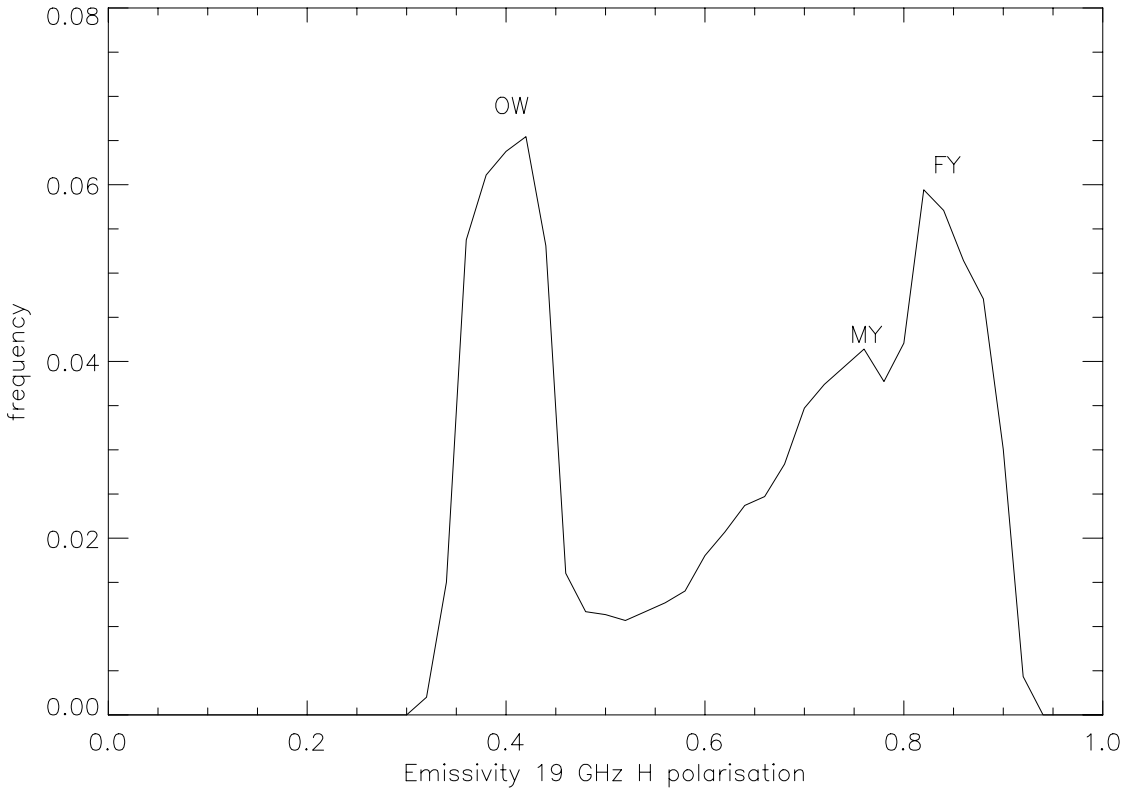

Fig. 3: Example of histogram from October 1997 off North East Greenland illustrating a mixture of FY, MY and OW.

3.2.1 Open water tiepoints

It is relatively simple to assess the OW tiepoints. They may be determined as the monthly mean value, hence reflecting the monthly mean (climatological) atmospheric water content and wind roughening as well as surface temperature. There is, of course, geographical variation in the climatological values of these constituents. However, the OW tiepoint primarily determines the position of the ice edge and the importance therefore lies in that vicinity. Consequently, the OW tiepoint is extracted at a close distance from the ice edge sufficient to guarantee ice free conditions.

3.2.2 Ice tiepoints

The ice tiepoints are somewhat more complicated to deal with, the main problems may be summarised as:

1) The presence of OW (leads and melt ponds) in the perennial ice.
2) The representativity of the sample chosen.

3) Purity of the sample ice type.

For FY, it is important to choose an area of ice that is known to be of 100 % concentration and located in the seasonal ice zone to avoid contamination with MY ice. To aid in locating such areas, a-priori knowledge along with images of PR_{19} are used in choosing gridcells characterised by minimum PR_{19} and the highest emissivity characterised by a peak in the histogram is selected as the tiepoint. During winter this is straightforward and the validity of the tiepoint rests on the assumption that the statistics of the 250x250 km grid cell are dominated by pixels of 100% ice concentration. This procedure is similar to the one adopted by Thomas, 1993.

During summer the ice is broken up and the surface is extensively covered by melt ponds. In addition the MY ice looses its characteristics and merges with the FY ice into a summer ice signature, rendering ice type analyses impossible [e.g. Comiso, 1983]. The ice emissivity during summer is very variable; it is determined by the extent of melt ponds that lead to decreased emissivity and wet snow cover effects that lead to increased emissivities. In addition come uncertainties in the extent of cracks and leads, however, previous studies show that ice concentrations during summer are very high, between 90 and 100% [Carsey, 1982; Campbell et al., 1984; Barry and Maslanik, 1989]. Melt ponds may affect up to 80 % of the sea ice surface [Grenfell and Lohanick, 1985] and is a fundamental problem that cannot be distinguished from leads or cracks. It will lead to seriously depressed ice concentrations if one chooses the overall maximum emissivity (that corresponds to wet snow) as tiepoint during summer. In order to reduce these effects we choose gridcells characterised by high PR_{19} to locate areas with a low extent of open water (i.e. cracks, leads and meltponding) and the mean emissivity within these cells to avoid the wet snow signature. This will of course lead to larger occurrences of total ice concentration estimates in excess of 100% during summer but the mean hemispheric concentration should remain closer to the true value.

By definition, the ice cover that is present by the fall freezeup is classified as MY. However, the MY tiepoint is even more problematic than the FY as old leads freeze up and yield an unknown mixture of OW, MY and FY. Furthermore there is evidence that the radiative properties of the MY ice itself is varying considerably over time, which gives rise to a lack of consistency in the retrieved MY ice coverage. The procedure for establishing the MY tiepoint is to use GR_{1937V} to enable the identification of gridcells of high MY concentration [Cavalieri and Gloersen, 1984]. Subsequently, the assessment of the tiepoint is based on use of histograms in conjunction with experience from previously published works [e.g. Svendsen et al., 1983; Comiso, 1983; Pedersen, 1991; Eppler et al., 1992; Steffen and Schweiger, 1991; Thomas, 1993]. For frequencies lower than 37 GHz and all V-polarised channels, a peak in the histogram located between the peaks associated with OW and FY represents MY. For H-polarised frequencies from 37 GHz and up, the emissivity of MY is less than that of OW, which simplifies the tiepoint extraction to that of the generally lowest emissivity peak within the MY ice pack.

In Figure 4 are shown typical examples of histograms used in the analysis. Although they represent the Arctic, histograms drawn from the Baffin Bay and the Baltic are quite similar. With the single peak it is extremely straightforward to establish the tiepoint and only in a couple of cases during the summer was it impossible to establish unambiguously the MY tiepoint. Fortunately, the same month and channel was not affected by this both years and the tiepoint could therefore be established.

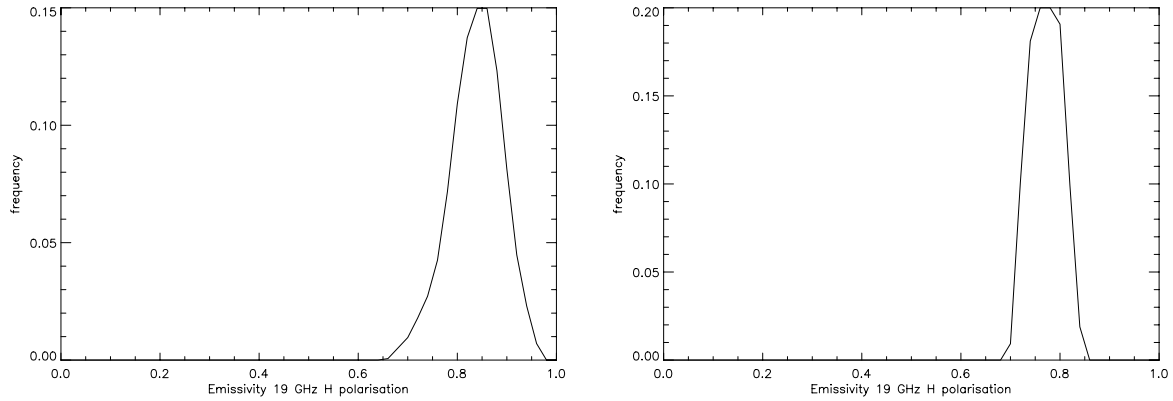

Fig. 4: Typical examples of histograms used to define tiepoints from October 1997. The left represents FY ice in the Kara Sea, the right panel represents MY ice off the Canadian Archipelago. Notice that in both cases the histogram contains only one peak, facilitating the determination of the tiepoints. Although this sample is drawn from the Arctic Ocean, similar histograms are obtained in the Baltic and in the Baffin Bay.

As can be seen from plates 1 and 2 (found in Appendix C), the Arctic ice season of 1996 was characterised by less extensive breakup than usual leaving large expanses of the Kara, Barents and Laptev Seas ice covered although they are usually ice free during summer. At the same time the East Coast of Greenland experienced very mild ice conditions. Accordingly, at the onset of freezing conditions in autumn of 1996 until the melt season of 1997, areas characterised by ice of large negative GR_{1937V} (MY signature) are found in a much wider area than usual. The summer of 1997 was much more typical as the Barents and Kara Seas this year were completely free of ice during the summer. At the onset of freezing the ice characterised by low GR_{1937V} is seen to retreat considerably towards the Canadian Archipelago. As a consequence of these conditions great care must be exercised when establishing the FY tiepoint after the summer of 1996 in order to avoid areas of 2'nd year ice. It is found, however, that areas of the Laptev, Kara and Barents Seas are characterised by GR_{1937V} close to zero, minimum PR_{19} as well as overall maximum emissivities which can be taken as strong evidence that there are in fact pixels within this area covered completely by FY ice. Consequently the Arctic FY tiepoint is taken from this general area.

In the Baffin Bay the ice usually melts completely during summer. However, in 1996 this was not the case and consequently MY ice might be found in a small area close to the Greenland Coast during the winter of 1996/1997. This leads to avoidance of the area closest to the Greenland Coast when establishing the FY tiepoint as it is most likely to contaminate the tiepoint with MY ice. Although the ice did not vanish completely, the widespread melt during July-September was found to destroy the possibility of establishing a credible tiepoint.

In the Baltic the ice melts completely during summer, hence it is not necessary to consider contamination of the FY signature with old ice. Rather it is the possible contamination by land that requires careful analysis to avoid introduction of artefacts. The ice extent is generally only sufficient to allow determination of tiepoints during the months from January through April.

4. Results

Following the methodology given in the previous section the set of tiepoints for the Arctic Ocean, the Baffin Bay and the Baltic were determined. The results are given in Tables 1-3 for the Arctic Ocean, Tables 4-5 for the Baffin Bay and Tables 6-7 for the Baltic. The Tables are found in Appendix A, while plots of the tiepoints can be found in Appendix B. Not surprisingly the difference in the tiepoint emissivity estimates between years was highest in the summer months attaining values as high as 0.06 for the 85H MY tiepoint during August. For the lower frequencies and for FY and OW tiepoints in general there was much better consistency from year to year. The maximum difference was 0.04, again in the month of August. Over all, a typical difference in emissivity was found to be about 0.01.

In the Arctic based on PR_{19} and GR_{1937V} all MY tiepoints were found in a well confined region North of the Canadian Archipelago. Similarly, the FY tiepoints were found in the Kara and Laptev Sea area, which is consistent with general knowledge of the Arctic ice climate. Figure P.1 found in Appendix B depicts the yearly variation of these tiepoint signatures. Note that the polarisation ratio for ice is relatively constant throughout the year for all channels and always in great contrast to the polarisation ratio for OW. During the winter months the tiepoints are generally in reasonable accordance with the emissivities measured during NORSEX (see Figure 1). One exception is the evolution of the MY tiepoint at 85 GHz that for several months is even higher than that for 37 GHz. This is in contrast to the NORSEX measurements and surprising as one would expect the increased scattering in MY to attenuate the emissivity of the 85 GHz channel. To investigate the nature of the phenomenon more closely images of monthly mean GR_{3785V} for 1996 and 1997 where negative values (corresponding to agreement with the NORSEX signatures) are masked out are presented in plate 3, see Appendix C. Hence, under normal circumstances one would expect the entire Arctic and MY areas in particular to be masked out during winter. However, the feature is seen to arise and spread from approximately February in what is known as areas of very old ice off the Canadian Archipelago. It vanishes abruptly in June to emerge again covering almost the entire Arctic from July through October. During the months of October through December 1997 the feature vanishes. However, during the same period of 1996 it remains and even affects the months of January through May of 1997. The origin of the phenomenon is not known to the author but may be connected with varying snow properties like e.g. ice crusts within the snow or salt contamination of the surface. It affects areas of MY and FY ice indiscriminately during summer/autumn, when the effect can probably be ascribed to the presence of liquid water on top of the ice. Thus, the signature is undoubtedly not associated with the same physical property in summer and winter.

On a more general level, at the onset of summer, it is evident that the tiepoint signatures are heavily affected by surface effects arising due to melt ponds and wetness of the snow cover and the polarisation ratio over ice is increased accordingly. Especially for July, the tiepoints reflect the total merging of the MY and FY signatures. The validity of the September FY tiepoints may be argued as the minimum ice extent is generally found to occur during that month [e.g. Comiso, 1990]. Accordingly, indications of OW contamination of the September FY tiepoint are evident in the generally increased polarisation ratio.

The Baffin Bay 19 and 37 GHz tiepoint emissivities (see Appendix B, Figure P.2) differ only slightly from those observed in the Arctic. The most notable distinction is probably that the minimum in PR_{37} found in both areas during October persists well into November in the Baffin Bay. At 85 GHz on the other hand large differences in the emissivity level are found

although PR_{85} is found to be relatively invariant. The polarisation ratio over ice in the Baltic (see Appendix B, Figure P.3) as compared to the two other areas is generally larger due to a relative depression in the level of the 19H and 37H channels and an increase in the 85V level. There are no apparent signs of land contamination.

As for OW, the horisontally polarised signatures are most sensitive to differences in the monthly wind and water vapour distributions between different locations. The overall emissivity differences between the Baltic, the North Atlantic and the Baffin Bay are marginal, which is in agreement with previous works [Pedersen, 1991; Ulaby et al., 1986].

In order to provide a reference atmospheric state, climatological values of wind and water vapour in the areas of interest are taken from Serreze et al. (1994) and are given in Table 8, see Appendix A. The monthly mean of cloud liquid water is assumed to be negligible. The small geographical differences in the climatological values of water vapour and wind are taken as confirmation of the low geographical variability also found in the OW tiepoints. To further substantiate the latter point, simulated brightness temperatures over open water are computed based on the climatological values given in Table 8. For that purpose the MWMOD Radiative Transfer Model [Fuhrhop, 1997] is used with effects of surface roughness represented following the parameterisation of Wisler and Hollinger, 1977. However, no claim is made of the absolute calibration of the model in this setup. The result is presented in Figure 5 where the solid line represents the relation of equation 1 assuming a surface temperature of 272 K. The dots represent simulated brightness temperatures based on the climatological atmospheric state associated with each tiepoint. The solid line is displaced from the simulated datapoints but the slope is similar, which indicates the lack of calibration of the Radiative Transfer Model, rather than disagreement. The general scatter in the simulated values is found to be equivalent to ± 0.01 in emissivity which corresponds approximately to the precision at which the tiepoints are established.

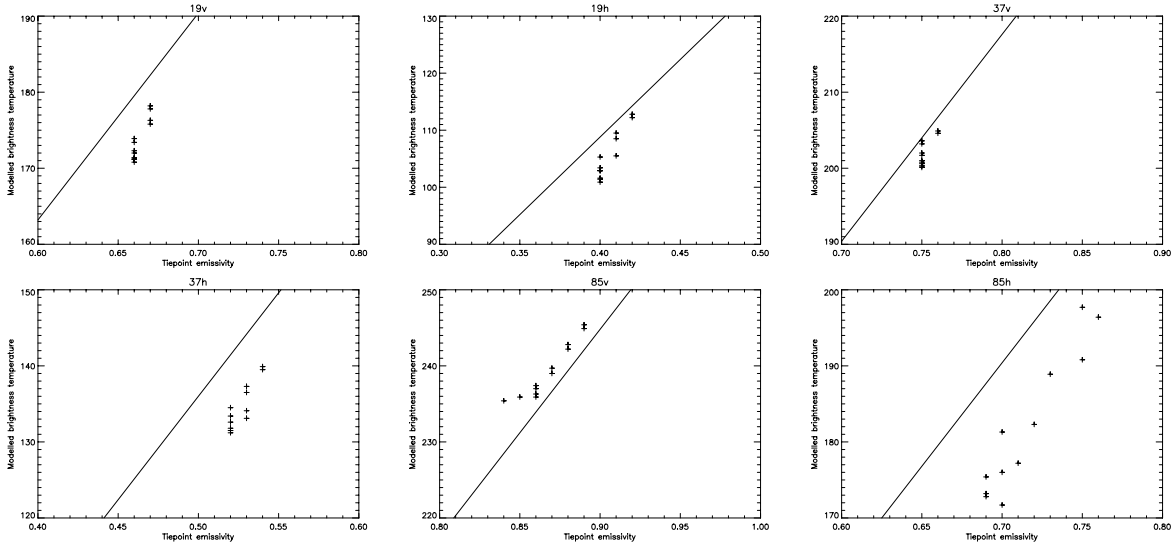

Fig. 5: Arctic OW Tiepoint emissivities vs. simulated brightness temperatures computed from monthly atmospheric climatology (Table 8). The full line represents brightness temperatures computed from tiepoint emissivities using equation 1 and assuming a water temperature of 272 K.

5. Discussion and conclusion

The tiepoints extracted here from the record of DMSP F-13 SSM/I measurements from 1996 and 1997 are generally quite close to those reported in earlier works based on field measurements or SMMR data [Pedersen, 1991; Comiso, 1983; Svendsen, 1983] for the 19 and 37 GHz channels. The 85 GHz channels, on the other hand, reveal marked differences from the NORSEX field measurements in all seasons. The unstable nature of the 85 GHz MY signature certainly complicates the use of these channels for MY ice retrieval.

The differences between summer- and winter months is relatively large for both MY and FY ice types although the largest variation is detected over MY. This has several reasons, such as a larger extent of meltponding over MY ice [Grenfell and Lohanick, 1985] and the fact that the occurrence of wet snow raises the emissivity of the MY type to be comparable to that of FY, while leaving the FY emissivity relatively unaffected. The breakdown of the separation between MY and FY ice comes both in 1996 and 1997 in July, while the emissivities for June are only slightly influenced. Note that for the month of July, where the emissivities of MY at 19 and 37 GHz increase abruptly the 85 GHz emissivities are practically unaffected. Except for July it is clearly possible to distinguish between two major ice types. The critical question in summer is whether or not it is true that substantial areas of 100% ice concentration with or without melt ponds exist. This is not clear at present but if it is true one should use the summer tiepoints. Otherwise an interpolation between June and October, thus ignoring wet snow and meltponds, might be more appropriate. Certainly, at the time of the minimum ice extent in September, FY ice is by definition practically nonexistent. The signature is accordingly smaller and more polarised indicating serious OW contamination. It is therefore recommended to at least replace the FY signature for September with an average of the August and October signatures. The advent and ending of the summer melt may be readily diagnosed using the methodology outlined by e.g. Smith (1998) to determine when to start using the high emissivity July tiepoint and when to revert to a lower one. It is unavoidable, however, that the summer concentration estimates will be much more uncertain than those of the cold seasons but the planned validation study may test some of the above aspects and assumptions.

The geographical differences are marginal between the Arctic and the Baffin Bay. As could be expected, however, the difference between the Arctic and the Baltic is larger and the Baltic FY emissivities are generally lower, which is in accordance with the lower salinity observed there. At 85 GHz, on the other hand, the V-polarised emissivity is higher while the H-polarised one is at approximately the same level as observed elsewhere.

The present study bears some implications for algorithm development. Plate 3 (see Appendix C) presents large interannual variations in the signature of MY at 85 GHz. This is clear evidence that it is presently not feasible to use the 85 GHz channel for ice type classifications. However, once the reasons for the observed behaviour is understood it might add interesting knowledge on other important aspects. It is observed that the polarisation ratio remains at a relatively constant level throughout the year and that the differences between MY and FY ice are small. This confirms the usefulness of the parameter for total ice concentration retrieval at 85 GHz as it is found by Svendsen et al. (1987). The much increased sensitivity to atmospheric noise, however, is still an unresolved issue [Lubin et al., 1997].

It is anticipated that the tiepoints presented here will be able to contribute to more exact retrievals of both FY and especially MY when used in conventional algorithms based on the

19 and 37 GHz channels. Furthermore it facilitates a more consistent accounting for the effects of the atmosphere as it allows the definition of a reference atmospheric state from climatology associated with each individual tiepoint. This is feasible due to the fact that in practice the tiepoints for each individual surface type are retrieved in a relatively well confined area from month to month. For completeness, total precipitable water, wind speed reduced to 10 m and surface pressure, extracted at representative locations from climatology [Serreze et al., 1994] are given in Table 8 and their consistency with the OW tiepoints is illustrated in Figure 5.

5.1 Recommendations

The present set of tiepoint have been determined to accommodate the use of auxiliary data for elimination of e.g. atmospheric effects and effects of surface temperature. For most months it is recommended that the tiepoints be interpolated linearly in time to avoid discontinuities in the retrieved concentrations at the turn of each month. The FY tiepoints for September do not seem valid and should therefore be replaced by an interpolation of the adjacent months. In the remaining summer months the ice tiepoint estimation may also suffer from water contamination in the form of cracks and leads. The extent is unknown and indistinguishable from melt ponds. However, as reference data on actual ice concentrations (with or without melt ponds) is needed, it is left to a planned ice algorithm validation study to assess the validity and usefulness of the remaining summer tiepoints. To assure and assess the validity of long term retrievals made with any kind of tiepoint set, the interannual variations in tiepoint emissivity should be assessed using a much longer dataset than the one used here.

6. Acknowledgements

The present report describes the outcome of work performed during the authors stay as a visiting scientist under the EUMETSAT SAF on Ocean and Sea Ice development project at the National/Naval Ice Center, Washington D.C. For assistance and fruitful discussion during the stay thanks are extended to Kim Partington and Adnan Trakic, NIC as well as Robert Grumbine, NCEP and Don Cavalieri, NASA GSFC. Leif Toudal Pedersen is thanked for providing valuable comments to the manuscript. NCEP Reanalysis data provided by the NOAA-CIRES Climate Diagnostics Center, Boulder, Colorado, from their Web site at http://www.cdc.noaa.gov/ is used in this work.

7. References

Barry, R.; J. Maslanik: Arctic sea ice characteristics and associated atmosphere - ice interactions in summer inferred from SMMR data and drifting buoys: 1979-1984, Geojournal, 18, 1, 1989.

Campbell, W. J.; P. Gloersen; H. J. Zwally: Aspects of Arctic sea ice observable by sequential passive microwave observations from the Nimbus-5 satellite, in I. Dyer and C. Chryssotomidis (Ed.): Arctic Technology and Policy, 197-122, Hemisphere, New York, 1984.

Cavalieri, D. J.; K. M. St. Germain; C. T. Swift: Reduction of weather effects in the calculation of sea-ice concentration with the DMSP SSM/I, J. Glaciol., 41, 139, 455-464, 1995.

Cavalieri, D. J.; P. Gloersen: Determination of sea ice parameters with the Nimbus 7 SMMR, J. Geophys. Res., 89, C4 , 5355-5369, 1984.

Comiso J.C.: Characteristics of Arctic winter sea ice from satellite multispectral microwave observations, J. Geophys. Res., 91, C1, 975-994, 1986.

Comiso, J. C.: Arctic multiyear ice classification and summer ice cover using passive microwave satellite data, J. Geophys. Res., 95, C8 , 13411-13422, 1990.

Comiso, J. C.: Sea ice effective microwave emissivities from satellite passive microwave and infrared observations, J. Geophys. Res., 88, C12, 7686-7704, 1983.

Eppler, D.; M. R. Anderson; D. J. Cavalieri; J. C. Comiso; P. Gloersen; C. Garrity; T. C. Grenfell; M. Hallikainen; J. A. Maslanik; C. Mätzler; R. A. Melloh; I. Rubinstein; C. Swift: Passive microwave signatures of sea ice. In Carsey (Ed.): Microwave remote sensing of sea ice, American Geophysical Union, Washington DC, 48-71, 1992.

Fuhrhop, R.: MWMOD user manual, Institut für Meereskunde, Christian-Albrechts-Universität, Kiel, Germany, 82 pp., 1997.

Gloersen, P.; D. J. Cavalieri: Reduction of weather effects in the calculation of sea ice concentration from microwave radiances, J. Geophys. Res., 91,C3 , 3913-3919, 1986.

Grenfell, T. C.; A. W. Lohanick: Temporal variations of the microwave signatures of sea ice during the late spring and early summer near Mould Bay NWT, J. Geophys. Res., 90, C3 , 5063-5074, 1985.

Heyster, G.; B. Burns; T. Hunewinkel; K. Künzi; L. Meyer-Lerbs; H. Schottmüller; C. Thomas; P. Lemke; T. Viehoff; J. Turner; S. Harangozo; T. Lachlan-Cope; L. T. Pedersen: Pelicon - Project for estimation of long term variability in ice concentration, Final report, EC Contract EV5V-CT93-0268 (DG 12 DTEE), 188 pp., 1996.

Lubin, D.; C. Garrity; R. O. Ramseier; R. H. Whritner: Total sea ice concentration retrieval from the SSM/I 85.5 GHz channels during the arctic summer. Remote Sens. Environ., 62, 63-76, 1997.

Oelke C.: Atmospheric signatures in sea-ice concentration estimates from passive microwaves: modelled and observed, Int. J. Remote Sensing, 18, 5, 1113-1136, 1997.

Parkinson C. L., J. C. Comiso, H. J. Zwally, D. J. Cavalieri, P. Gloersen, W. J. Campbell: Arctic sea ice, 1973-1976: Satellite passive microwave observations, NASA-SP-489, 296 pp., 1987.

Pedersen, L. T.: Retrieval of sea ice concentration by means of passive microwave radiometry, PhD dissertation LD 81, Electromagnetics Institute, Technical University of Denmark, 148 pp., 1991.

Rothrock D. A., D. R. Thomas, A. S. Thorndike: Principal component analysis of satellite passive microwave data over sea ice, J. Geophys. Res., 93, C3, 2321-2332, 1988.

Serreze M. C., M. C. Rehder, R. G. Barry, and J. D. Kahl: A climatological data base of Arctic water vapor characteristics. Polar Geography and Geology, 18, 63-75, 1994.

Smith D. M.: Recent increase in the length of the melt season of perennial Arctic sea ice, Geophysical Research Letters, 25, 5, 655-658, 1998

Steffen K.; A. Schweiger: NASA Team algorithm for sea ice concentration retrieval from Defense Meteorological Satellite Program Special Sensor Microwave Imager: Comparison with Landsat imagery. J. Geophys. Res., 96, C12, 21971-21987, 1991.

Svendsen E.; K. Kloster; B. Farelly; O. M. Johannesen; J. A. Johannesen; W. J. Campbell; P. Gloersen; D. J. Cavalieri; C. Mätzler: Norwegian remote sensing experiment: Evaluation of the Nimbus 7 scanning multichannel microwave radiometer for sea ice research. J. Geophys. Res., 88, C5, 2781-2791, 1983.

Svendsen E.; C. Mätzler; T. C. Grenfell: A model for retrieving total sea ice concentration from spaceborne dual-polarised passive microwave instrument operating near 90 GHz. Int. J. Remote Sensing, 8, 10, 1479-1487, 1987.

Thomas D. R.: Arctic sea ice signatures for passive microwave algorithms, J. Geophys. Res., 98, C6, 10037-10052, 1993.

Ulaby F. T., R. K. Moore, A. K. Fung: Microwave remote sensing active and passive, vol. III: From theory to application, Artech House, Norwood, MA, 1986.

Wensnahan M., G. A. Maykut, T. C. Grenfell, D. P. Winebrenner: Passive microwave remote sensing of thin sea ice using principal component analysis, J. Geophys. Res., 98, C7, 12453-12468, 1993.

Wentz, F.J.: Model function for ocean microwave brightness temperatures, J. Geophys. Res., 88, C3, 1892-1908, 1983.

Wilheit T. T., J. Blinn, W. Campbell, A. Edgerton, W. Nordberg: Aircraft measurements of microwave emissions from Arctic sea ice, Remote Sens. Eviron., 2, 129, 1972.

Wisler M. M., J. P. Hollinger: Estimation of marine environmental parameters using passive microwave radiometric remote sensing systems, Technical Report NRL Memo Rep. 3661, Naval Research Laboratory, Washington D.C., 1977.

Zwally H. J., J. C. Comiso, C. L. Parkinson, W. J. Campbell, F. D. Carsey: Antarctic sea ice, 1973-1976: Satellite passive-microwave observations, NASA-SP-459, 216 pp., 1983.

Appendix A: Tables

FY	Jan	Feb	Mar	Apr	May	Jun	Jul	Aug	Sep	Oct	Nov	Dec
19V	0,95	0,94	0,95	0,95	0,96	0,96	0,93	0,90	0,88	0,95	0,96	0,94
19H	0,89	0,89	0,90	0,89	0,89	0,91	0,87	0,87	0,84	0,87	0,91	0,89
37V	0,92	0,92	0,91	0,92	0,93	0,94	0,92	0,92	0,88	0,92	0,94	0,91
37H	0,89	0,88	0,88	0,88	0,88	0,89	0,86	0,85	0,78	0,88	0,89	0,88
85V	0,84	0,89	0,84	0,84	0,86	0,87	0,85	0,82	0,84	0,84	0,88	0,82
85H	0,82	0,84	0,83	0,82	0,84	0,83	0,83	0,77	0,74	0,76	0,83	0,78

MY	Jan	Feb	Mar	Apr	May	Jun	Jul	Aug	Sep	Oct	Nov	Dec
19V	0,83	0,83	0,84	0,85	0,86	0,87	0,94	0,81	0,81	0,83	0,83	0,84
19H	0,76	0,77	0,77	0,78	0,79	0,80	0,88	0,74	0,72	0,76	0,75	0,76
37V	0,70	0,71	0,71	0,72	0,75	0,78	0,93	0,67	0,71	0,72	0,71	0,70
37H	0,65	0,66	0,66	0,67	0,69	0,72	0,88	0,63	0,66	0,67	0,66	0,66
85V	0,67	0,69	0,72	0,75	0,77	0,80	0,77	0,74	0,74	0,73	0,75	0,70
85H	0,65	0,66	0,66	0,71	0,74	0,74	0,75	0,72	0,72	0,71	0,72	0,67

OW	Jan	Feb	Mar	Apr	May	Jun	Jul	Aug	Sep	Oct	Nov	Dec
19V	0,66	0,66	0,66	0,66	0,66	0,67	0,67	0,67	0,67	0,66	0,66	0,66
19H	0,40	0,40	0,40	0,40	0,40	0,41	0,42	0,42	0,41	0,41	0,40	0,40
37V	0,75	0,75	0,75	0,75	0,75	0,76	0,76	0,76	0,75	0,75	0,75	0,74
37H	0,52	0,52	0,52	0,52	0,52	0,53	0,54	0,54	0,53	0,53	0,52	0,52
85V	0,84	0,85	0,86	0,86	0,87	0,88	0,89	0,89	0,88	0,87	0,86	0,86
85H	0,70	0,69	0,69	0,70	0,70	0,73	0,75	0,76	0,75	0,72	0,71	0,69

Tables 1-3: Tiepoint emissivities for FY, MY and OW measured over or in the vicinity of the Arctic Ocean.

FY	Jan	Feb	Mar	Apr	May	Jun	Jul	Aug	Sep	Oct	Nov	Dec
19V	0,95	0,94	0,94	0,95	0,96	0,93				0,95	0,96	0,96
19H	0,89	0,90	0,90	0,90	0,88	0,85				0,89	0,89	0,90
37V	0,92	0,92	0,91	0,91	0,93	0,91				0,93	0,94	0,94
37H	0,88	0,88	0,88	0,87	0,88	0,84				0,91	0,90	0,89
85V	0,85	0,86	0,86	0,86	0,84	0,85				0,87	0,87	0,89
85H	0,83	0,83	0,83	0,83	0,81	0,81				0,81	0,82	0,85

OW	Jan	Feb	Mar	Apr	May	Jun	Jul	Aug	Sep	Oct	Nov	Dec
19V	0,66	0,66	0,66	0,66	0,66	0,67	0,68	0,67	0,67	0,66	0,66	0,66
19H	0,39	0,40	0,40	0,40	0,40	0,41	0,43	0,43	0,41	0,41	0,40	0,40
37V	0,75	0,75	0,75	0,75	0,75	0,76	0,77	0,76	0,75	0,75	0,75	0,74
37H	0,52	0,52	0,52	0,52	0,53	0,53	0,55	0,54	0,53	0,53	0,52	0,51
85V	0,84	0,85	0,86	0,86	0,87	0,88	0,90	0,89	0,88	0,87	0,86	0,86
85H	0,70	0,69	0,69	0,70	0,70	0,73	0,77	0,77	0,75	0,72	0,71	0,69

Tables 4-5: Tiepoint emissivities for FY ice and OW measured over the Baffin Bay.

FY	Jan	Feb	Mar	Apr	May	Jun	Jul	Aug	Sep	Oct	Nov	Dec
19V	0,93	0,93	0,94	0,94								
19H	0,83	0,84	0,85	0,85								
37V	0,92	0,91	0,91	0,89								
37H	0,83	0,82	0,83	0,82								
85V	0,91	0,92	0,89	0,88								
85H	0,84	0,81	0,82	0,82								

OW	Jan	Feb	Mar	Apr	May	Jun	Jul	Aug	Sep	Oct	Nov	Dec
19V	0,66	0,66	0,66	0,66								
19H	0,40	0,40	0,41	0,40								
37V	0,75	0,75	0,75	0,75								
37H	0,52	0,52	0,51	0,52								
85V	0,84	0,86	0,86	0,86								
85H	0,70	0,69	0,70	0,70								

Tables 6-7: Tiepoint emissivities for FY ice and OW measured over the Baltic Sea during the ice seasons of 1996 and 1997.

Arctic		Jan	Feb	Mar	Apr	May	Jun	Jul	Aug	Sep	Oct	Nov	Dec
FY	**PW**	2,00	2,03	2,26	3,10	5,69	10,35	13,90	12,41	8,50	4,34	2,72	2,26
MY	**PW**	1,79	1,59	1,78	2,46	4,80	9,16	12,33	10,91	7,11	3,45	2,17	1,90
OW	**PW**	4,77	5,28	5,24	6,37	8,29	11,71	15,06	14,44	12,36	9,21	6,71	5,28
	MW	1,00	-1,10	-0,57	-0,30	-0,20	0,17	-0,30	-0,57	0,00	-0,17	0,13	0,93
	ZW	-1,03	-0,53	-1,47	1,33	-1,40	-0,10	0,27	0,16	-0,40	-0,20	-1,50	-2,87
Baffin		**Jan**	**Feb**	**Mar**	**Apr**	**May**	**Jun**	**Jul**	**Aug**	**Sep**	**Oct**	**Nov**	**Dec**
FY	**PW**	2,45	2,35	3,07	3,36	5,62	9,80	13,49	11,94	9,42	5,10	3,46	2,78
OW	**PW**	3,07	3,04	4,15	4,89	7,44	13,28	18,59	15,83	12,31	7,01	4,78	3,67
	MW	-0,51	0,07	0,16	0,02	0,05	0,10	-0,47	0,02	0,07	0,09	-0,12	0,09
	ZW	1,87	1,43	1,09	-0,25	-1,15	-1,25	-1,45	-1,06	0,55	-0,05	1,00	1,41

Table 8: Precipitable water (PW) in mm, zonal wind (ZW) and meridional wind (MW) in m/s from climatology [Serreze et al., 1994] in areas representative to the tiepoint extraction.

Appendix B: Tiepoint plots

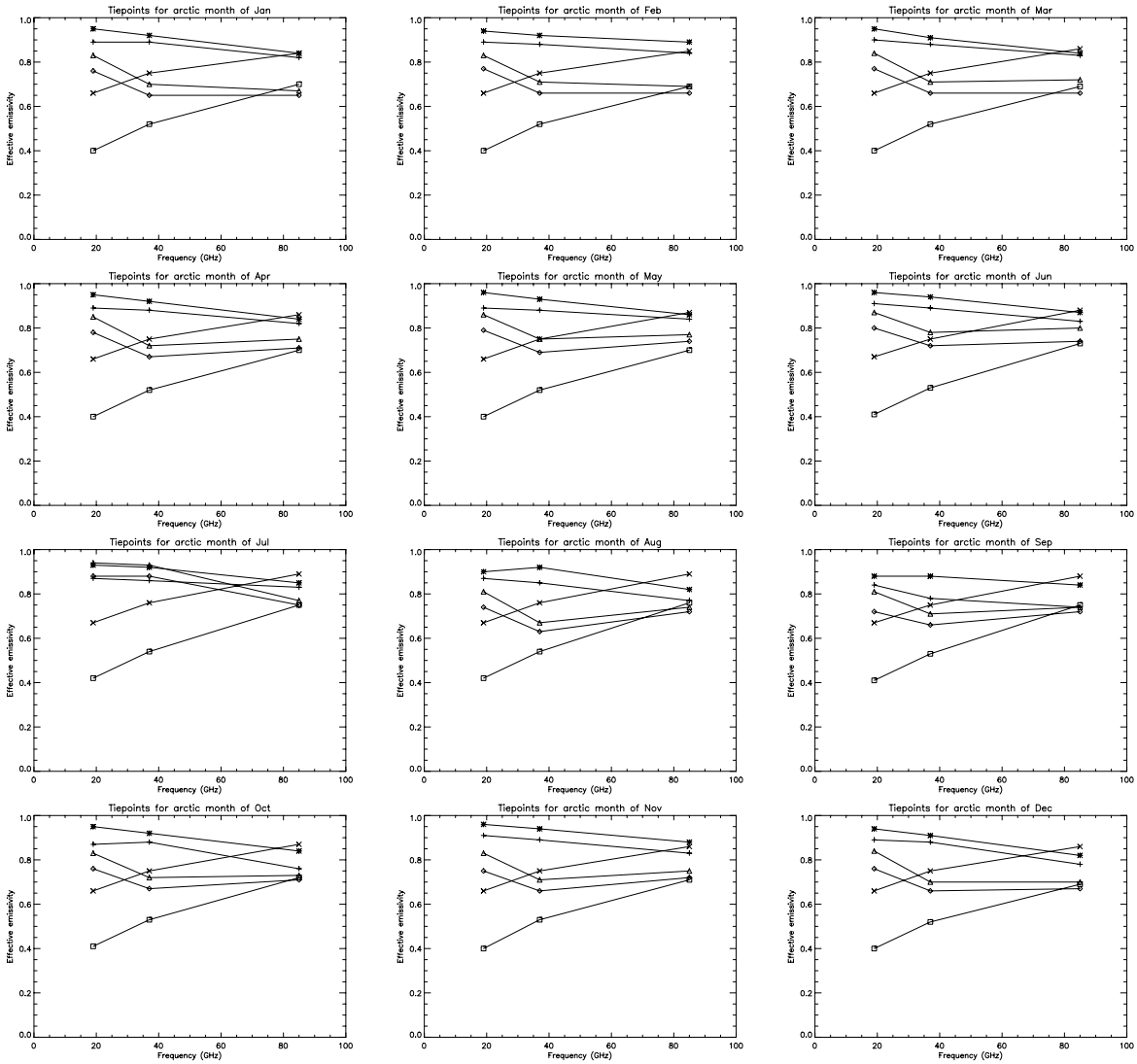

P.1: Graphic presentation of monthly tiepoint signatures for the Arctic Ocean. (*) V pol. FY, (+) H pol. FY, (Δ) V pol. MY, (✧) H pol. MY, (x) V pol. OW, (□) H pol. OW.

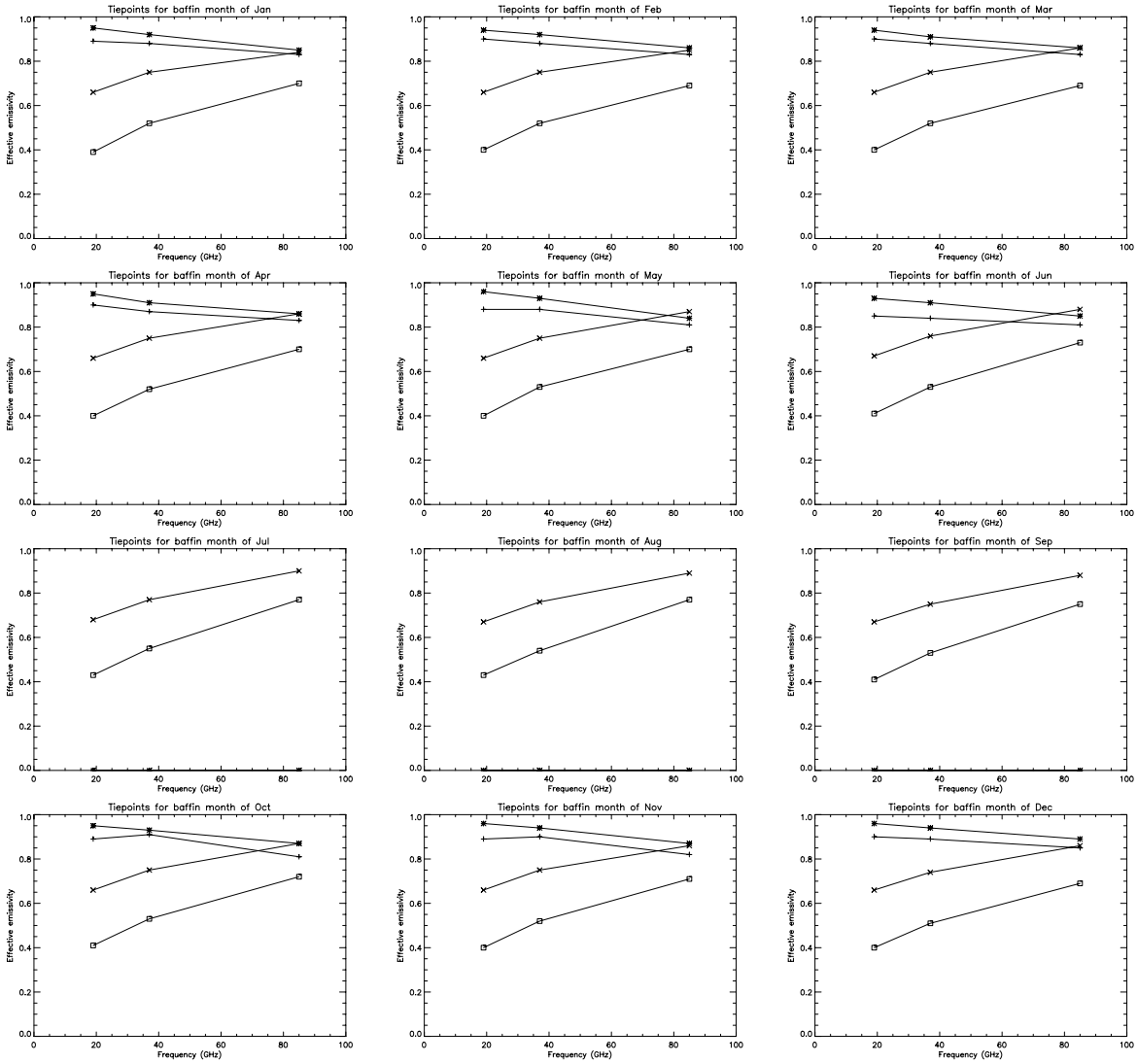

P.2: Graphic presentation of monthly tiepoint signatures for the Baffin Bay. (*) V pol. FY, (+) H pol. FY, (x) V pol. OW, (□) H pol. OW.

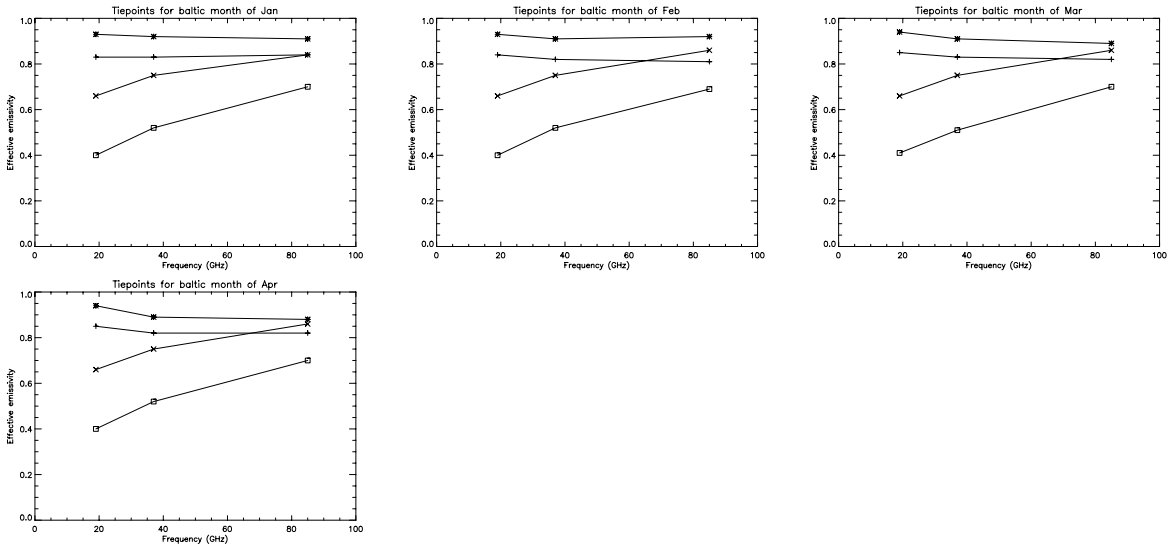

P.3: Graphic presentation of monthly tiepoint signatures for the Baltic Sea. (*) V pol. FY, (+) H pol. FY, (x) V pol. OW, (□) H pol. OW.

Appendix C: Plates

Plate 1: Maps of PR_{19} for 1996-1997.

Plate 2: Maps of GR_{1937V} illustrating the good correspondance with known MY areas during winter and the breakdown of the MY signature during summer.

Plate 3: Maps of monthly mean GR_{3785V} during 1996 and 1997.